Virology 427 (2012) 177–188

Contents lists available at SciVerse ScienceDirect

Virology

journal homepage: www.elsevier.com/locate/yviro

Structural evolution of the P22-like phages: Comparison of Sf6 and P22 procapsid and virion architectures

Kristin N. Parent [a], Eddie B. Gilcrease [b], Sherwood R. Casjens [b,*], Timothy S. Baker [a,c,**]

[a] University of California, San Diego, Department of Chemistry & Biochemistry, La Jolla, CA 92093, USA
[b] University of Utah School of Medicine, Division of Microbiology and Immunology, Department of Pathology, Salt Lake City, UT 84112, USA
[c] University of California, San Diego, Division of Biological Sciences, La Jolla, CA 92093, USA

ARTICLE INFO

Article history:
Received 11 November 2011
Returned to author for revision
10 January 2012
Accepted 30 January 2012
Available online 3 March 2012

Keywords:
cryoEM
Image reconstruction
Bacteriophage Sf6
Virus assembly
Procapsid
Virion

ABSTRACT

Coat proteins of tailed, dsDNA phages and in herpesviruses include a conserved core similar to the bacteriophage HK97 subunit. This core is often embellished with other domains such as the telokin Ig-like domain of phage P22. Eighty-six P22-like phages and prophages with sequenced genomes share a similar set of virion assembly genes and, based on comparisons of twelve viral assembly proteins (structural and assembly/packaging chaperones), these phages are classified into three groups (P22-like, Sf6-like, and CUS-3-like). We used cryo-electron microscopy and 3D image reconstruction to determine the structures of Sf6 procapsids and virions (~7 Å resolution), and the structure of the entire, asymmetric Sf6 virion (16-Å resolution). The Sf6 coat protein is similar to that of P22 yet it has differences in the telokin domain and in its overall quaternary organization. Thermal stability and agarose gel experiments show that Sf6 virions are slightly less stable than those of P22. Finally, bacterial host outer membrane proteins A and C were identified in lipid vesicles that co-purify with Sf6 particles, but are not components of the capsid.

Published by Elsevier Inc.

Introduction

The polypeptide backbones of the major coat proteins (CPs) of eukaryotic viruses and bacteriophages adopt a small number of unique folds, which is noteworthy since viral pathogens infect hosts in all kingdoms of life. Conservation of CP fold suggests that the assembly of viable virus shells is tightly controlled by a small set of specific conformations and inter-subunit interactions. The CPs are the protein building blocks that form the icosahedral and prolate shells of tailed, dsDNA-containing bacteriophages and members of the eukaryotic *Herpesviridae* family such as herpes simplex virus 1 (HSV-1), and these CPs share the "HK97-core" fold. This refers to the structure adopted by the 282 residue CP of bacteriophage HK97 (Fig. 1A, PDB ID 1OHG), whose capsid structure was the first of any tailed bacteriophage to be solved by X-ray crystallography (Wikoff et al., 2000). CPs with this fold often share 10–15% or less sequence identity, yet they exhibit several common features. These include a long (~20–30 a.a.) "spine helix"; an N-arm domain that can have α-helical content; a long, two-stranded β-sheet P-domain; and an A-domain with 4–6 loops and 2–4 helices and sometimes with 1–3 β-strands. Some HK97-like CPs have evolved an additional, surface-exposed protrusion that often consists of an Ig-like domain (Bamford et al., 2005; Morais et al., 2005; Parent et al., 2010a). The major CP of HSV-1 (1374 a.a.) displays even more elaborate additions to its HK97-core (Baker et al., 2005; Bamford et al., 2005). Thus, extensive surface modifications can be tolerated without compromising the ability of these proteins to assemble into functional virions. All viruses with HK97-like CPs assemble into intermediate, precursor structures called "procapsids". The genome is packaged into these procapsids, and in the case of tailed phages this is followed by the addition of the tail machinery.

P22, a dsDNA bacteriophage (family *Podoviridae*), has long served as an informative model system for exploring how phages and viruses utilize this basic assembly strategy (Casjens and Weigele, 2005; Prevelige, 2006; Prevelige and King, 1993; Teschke and Parent, 2010). There are currently 86 members of the P22-like phage group that have syntenic and largely homologous sets of twelve essential virion assembly genes. Casjens and Thuman-Commike (2011) classified the CPs of these "closely related" phages into three distinct types represented by P22 (Zinder and Lederberg, 1952), Sf6 (Gemski et al., 1975), and CUS-3 (Casjens and Thuman-

Abbreviations: a.a., amino acid, cryoEM, cryo electron microscopy; CP, coat protein; 3D, three-dimensional; gp, gene product; omp, outer membrane protein.

* Correspondence to: S.R. Casjens, Rm 2200 EEJMRB, Department of Pathology, University of Utah School of Medicine, Salt Lake City, UT 84112, USA. Fax: +1 801 585 2417.
** Correspondence to: T.S. Baker, Dept. of Chemistry & Biochemistry, University of California, San Diego, 9500 Gilman Drive MC-0378, La Jolla, CA 92093-0378, USA. Fax: +1 858 534 5846.
E-mail addresses: sherwood.casjens@path.utah.edu (S.R. Casjens), tsb@ucsd.edu (T.S. Baker).

0042-6822/$ – see front matter. Published by Elsevier Inc.
doi:10.1016/j.virol.2012.01.040

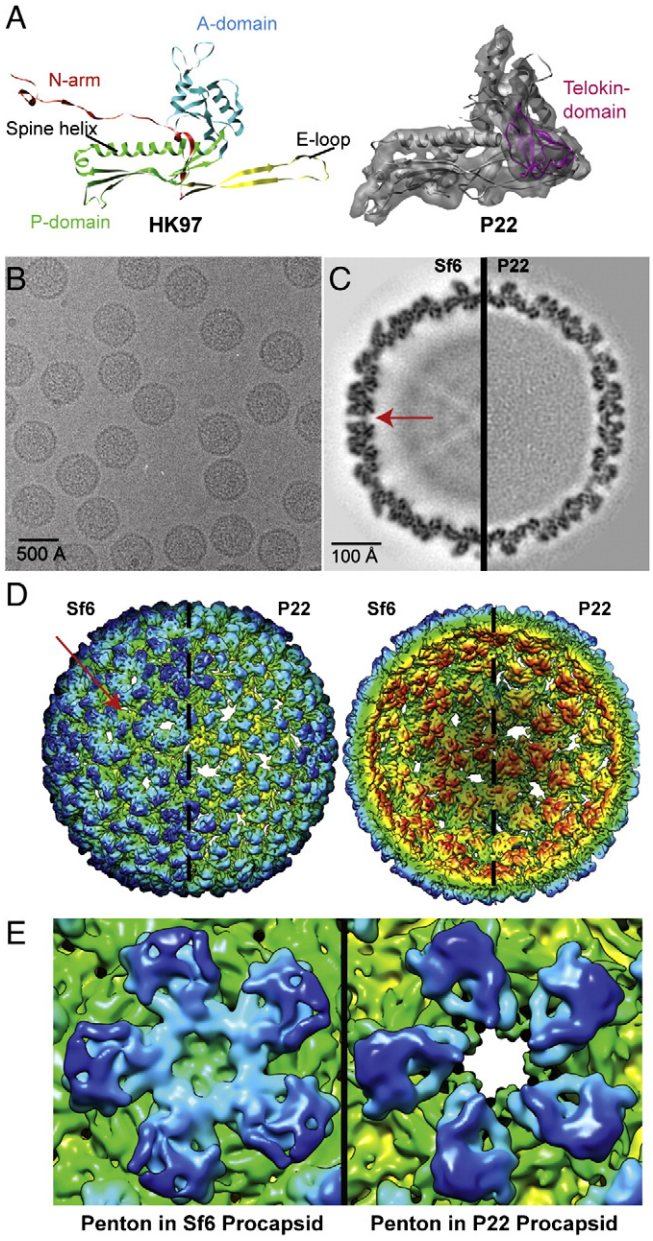

Fig. 1. 3D cryo-reconstructions of Sf6 and P22 procapsids. A. (Left) Ribbon diagram of HK97 CP (PDB ID 1OHG) color-coded to highlight domain organization. (Right) Segmented density for one CP subunit from the P22 procapsid cryo-reconstruction (transparent gray density, EMDB ID 5150) with a fitted ribbon diagram from the pseudo-atomic model of the P22 CP (PDB ID 3IYH) (Parent et al., 2010a). The telokin domain (absent in HK97) is highlighted in magenta. The HK97 and P22 subunit models are aligned with respect to their spine helices. B. Micrograph of an unstained, vitrified sample of Sf6 procapsids. C. Equatorial slabs (1 pixel, or ~1 Å thick) through the Sf6 (left half) and P22 (right half) procapsid density maps (features of highest and lowest density are depicted in black and white, respectively). The red arrow points to a solvent accessible channel in the Sf6 procapsid. D. Radially color-cued, surface representations of the Sf6 and P22 procapsid structures. For clarity, only the front (left pair) and back (right pair) quadrants of each structure are shown. The view direction in each pair is along an icosahedral two-fold axis of symmetry. Scale bar in panel (C) also refers to panel (D). E. Close-ups of the penton in Sf6 (left) and in P22 (right), each viewed along an icosahedral five-fold axis. The density maps in panels D and E were scaled and rendered at the same threshold, which highlights the closed verses open axial channels in Sf6 and P22, respectively.

Commike; King et al., 2007). However, the assembly pathway and virion structure have only been studied in detail for P22 (Casjens and Thuman-Commike, 2011; Prevelige, 2006). In this study, we

Table 1
Sf6 and P22 virion assembly proteins.

Gene product		Common name	Residues		% identity[a]
Sf6	P22		Sf6	P22	
1	3	Small terminase subunit	140	162	12
2	2	Large terminase subunit	470	499	15
3	1	Portal protein	708	725	30
4	8	Scaffolding protein	294	303	15
5	5	Coat protein	423	430	14
7	4	Tail protein	160	166	35
8	10	Tail protein	472	472	93
9	26	Tail needle	282	233	35
11	7	Ejection protein	230	229	82
12	20	Ejection protein	431	471	33
13	16	Ejection protein	665	609	32
14	9	Tailspike-endorhamnosidase	623	667	25

[a] Some values from Casjens and Thuman-Commike (2011).

determined the structures of Sf6 procapsids and virions. Most of the assembly proteins of Sf6 have amino acid sequences that are quite divergent from those of P22 (Table 1) (Casjens et al., 2004). For example, the large terminase subunits, portal proteins, and CPs of P22 and Sf6 share only about 15%, 30%, and 14% identity, respectively. High-resolution, X-ray crystallographic structures have been determined for three of the twelve Sf6 virion assembly proteins. These include the receptor-binding domain of the tailspike protein (gp14) (Muller et al., 2008), the small terminase (gp1) (Zhao et al., 2010), and the knob domain of the tail needle (gp9) (Bhardwaj et al., 2011).

Many phages, including Sf6, encode virulence factors that are expressed from the prophage in bacteria (Boyd and Brussow, 2002; Canchaya et al., 2004; Casjens and Hendrix, 2005; Cheetham and Katz, 1995). These factors can increase the fitness of the host by changing its surface characteristics, such as, for example, by affecting the composition of the external lipopolysaccharide layer (Allison and Verma, 2000; Banks et al., 2002; Broadbent et al., 2010). Such alterations can protect the bacterium from attack by other bacteriophages or the eukaryotic host's immune system. Sf6 infects the human pathogen, *Shigella flexneri*, and, in the prophage state it affects the host's pathogenicity by encoding an acetylase that alters the external O-antigen polysaccharide (Clark et al., 1991; Verma et al., 1991). *Shigella* cause bacillary dysentery ("shigellosis"), and some strains cause 10–15% fatality. *Shigella* includes four subgroups (Liu et al., 2008), and the most frequent isolate, *S. flexneri*, is present in ~60% of shigellosis cases (Yang et al., 2005). Transmission of *S. flexneri* occurs via the fecal–oral route and ~165 million cases occur annually (Kotloff et al., 1999). Bacillary dysentery typically affects children, but individuals with compromised immune systems such as AIDS patients are highly susceptible to *S. flexneri* infection (Kotloff et al., 1999). *Shigella* is quite virulent, as evidenced by the striking statistic that ingestion of as few as 10 bacteria is sufficient to induce shigellosis. The fact that Sf6 interaction with *S. flexneri* could result in a more dangerous human pathogen is a stimulus to investigate it in more detail.

In this study we have used cryo-electron microscopy (cryoEM) and three-dimensional (3D) image reconstruction to explore Sf6 virion structure and assembly. We computed icosahedrally-symmetrized cryo-reconstructions of Sf6 procapsids and mature particles at subnanometer resolutions. In addition, we determined the structure of the entire, asymmetric Sf6 virion at a moderate resolution (~16 Å). We show that Sf6 has a "tail machine" and extended portal "barrel" quite similar to P22 (Olia et al., 2011; Tang et al., 2011). Furthermore, the Sf6 CP has the conserved, HK97-like core and a surface-exposed, telokin domain (Fig. 1A). Despite showing overall morphological similarity, the CPs of Sf6 and P22 exhibit distinct differences in tertiary

structure and inter-subunit contacts, and the Sf6 capsid is slightly less stable than that of P22.

Results

Sf6 procapsid structure

Sf6 procapsids harvested from phage-infected cells (see Materials and methods) were vitrified and imaged under standard cryoEM conditions (Fig. 1B) (Baker et al., 1999). Image preprocessing and icosahedral reconstruction methods were performed as described by Parent et al. (2010a). In brief, 139 transmission electron micrographs were recorded, and 6851 particle images were included in the final 3D reconstruction at an estimated resolution of 7.8 Å (Table 2). Density for procapsid components that do not strictly follow the icosahedral symmetry of the CP, such as the portal protein complex, the ejection proteins, and all or most of the scaffolding proteins, was reduced to an insignificant level in the cryo-reconstruction as a result of the icosahedral averaging imposed during the image processing procedures. The gross morphology of the Sf6 procapsid is quite similar to the P22 procapsid shell that lacks scaffolding protein (EMDB ID 5149) (Parent et al., 2010a) and both exhibit T = 7 *laevo* symmetry. Sf6 and P22 CP shells are similar in diameter and their CPs both have a distinct protrusion on the outer surface. The CPs in both shells are organized as oligomers ("capsomers"), 12 of which are pentamers ("pentons") and 60 of which are hexamers ("hexons") (Fig. 1D). Hexons of the Sf6 procapsid are skewed significantly and exhibit two-fold rather than six-fold symmetry. This hexon skewing is similar to that seen in P22 (Thuman-Commike et al., 1996), T7 (Agirrezabala et al., 2005), λ (Dokland and Murialdo, 1993), HK97 (Conway et al., 1995), 80α (Spilman et al., 2011), and HSV-1 (Trus et al., 1996). Though the Sf6 and P22 procapsids share many common structural features, closer inspection of the details of the cryo-reconstructions reveals numerous, significant differences.

The Sf6 procapsid cryo-reconstruction contains many tube-shaped density features, consistent with the presence of α-helical secondary structural elements. These and other clearly-defined features indicate that the CP subunits of Sf6 have an HK97-like core, but the overall shape and tertiary structure of the subunit differs from that seen in the P22 procapsid (Figs. 2A and B). For example, when the Sf6 and P22 procapsid CP structures were aligned with respect to the spine helices, two distinct differences became obvious. First, the Sf6 P-domain has inter-capsomer contacts at the icosahedral two-fold symmetry axes that are far less extensive than those in P22. Second, the surface-exposed, telokin domain in Sf6 adopts a different orientation relative to that seen in P22, and this results in quite extensive, intra-capsomer subunit contacts (between telokin domains) that are absent in P22.

Substantial differences in the quaternary structures of Sf6 and P22 procapsids are evident in radial density projections (Fig. 3). For example, these show the disposition of the high radius, CP protrusions in pentons (r = 297 Å) and hexons (r = 283 Å). In Sf6, the telokin domains adopt a different rotational orientation compared to P22, which results in dramatic changes in intra-capsomer contacts (r = 275 Å). As a consequence, the axial hole in Sf6 hexons is smaller than that in P22 (Fig. 2), and the penton is completely closed in Sf6 but is open in P22. The latter difference, however, is more likely attributed to changes in the A-domain than to changes in telokin orientations (Figs. 1E and 2).

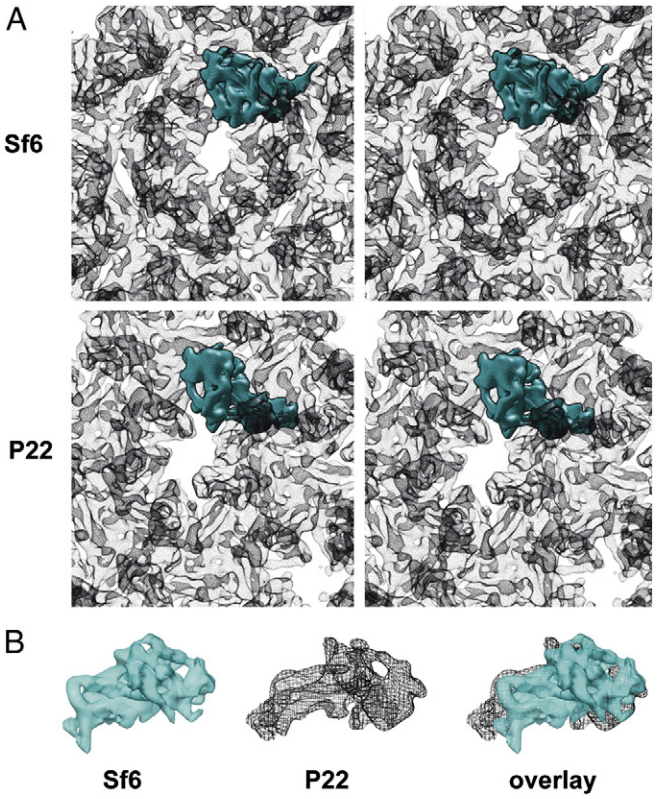

Fig. 2. The folds of Sf6 and P22 CPs are similar. A. Stereo views of hexons in Sf6 and P22 procapsids with the density envelope of a single subunit in each highlighted in cyan. B. Segmented density envelopes of individual CPs from Sf6 (cyan, solid density) and P22 (black mesh), and the two aligned with respect to the spine helices and superimposed using Chimera (Goddard et al., 2007).

Substantial differences in inter-capsomer contacts between Sf6 and P22 create a more porous shell in Sf6, and this is especially evident at the interfaces between hexons at both the local and strict two-fold axes of symmetry (Figs. 1D and 2). However, contacts between Sf6 subunits are most extensive at the quasi- and strict three-fold axes of symmetry as was observed in P22, where it was hypothesized to be a major contributor to overall capsid stability (Parent et al., 2010a). Lastly, the putative N-terminal arm domain and spine helix in Sf6, when compared to P22, lie at a steeper angle to the inner surface of the capsid shell and protrude further towards the particle center (Figs. 1E and 3, r = 242 Å).

P22 scaffolding protein is recycled through multiple rounds of procapsid assembly (Casjens et al., 1985; King and Casjens, 1974), and after each round intact scaffolding protein likely exits via the axial holes in CP hexons during maturation (Prasad et al., 1993). It is not yet known if Sf6 scaffolding protein is recycled like that of P22 or whether it might be proteolyzed during maturation. Scaffolding proteins are removed by proteolysis in many phages, but in those cases a recognizable protease gene is carried by the phage. There is no evidence for a protease gene in Sf6 or an autoproteolysis region of its scaffolding protein (Casjens et al., 2004). Although the holes in Sf6 procapsid shells are not as large as those of P22, they are more porous than HK97 and HSV-1, which proteolyze their scaffolds (Brown and Newcomb, 2011; Huang et al., 2011). Therefore, we predict that the Sf6 scaffolding protein will exit the procapsid intact and be recycled. Little if any density inside of the Sf6 procapsid

Table 2
Reconstruction statistics.

Symmetry applied	Sample	Micrographs	Images[a]	Defocus (μm)[b]	Pixel size (Å)	Resolution (Å)[c]
532	Procapsids	139	6851	0.58–4.61	1.07	7.8
532	Virions	469	15,483	0.53–3.95	1.07	7.0
1	Virions	611	16,253	0.10–4.61	2.14	16.0

[a] Number of boxed particles used in each image reconstruction.
[b] Range of objective lens underfocus settings for micrographs.
[c] Estimation based on $FSC_{0.5}$ criterion (van Heel and Schatz, 2005.)

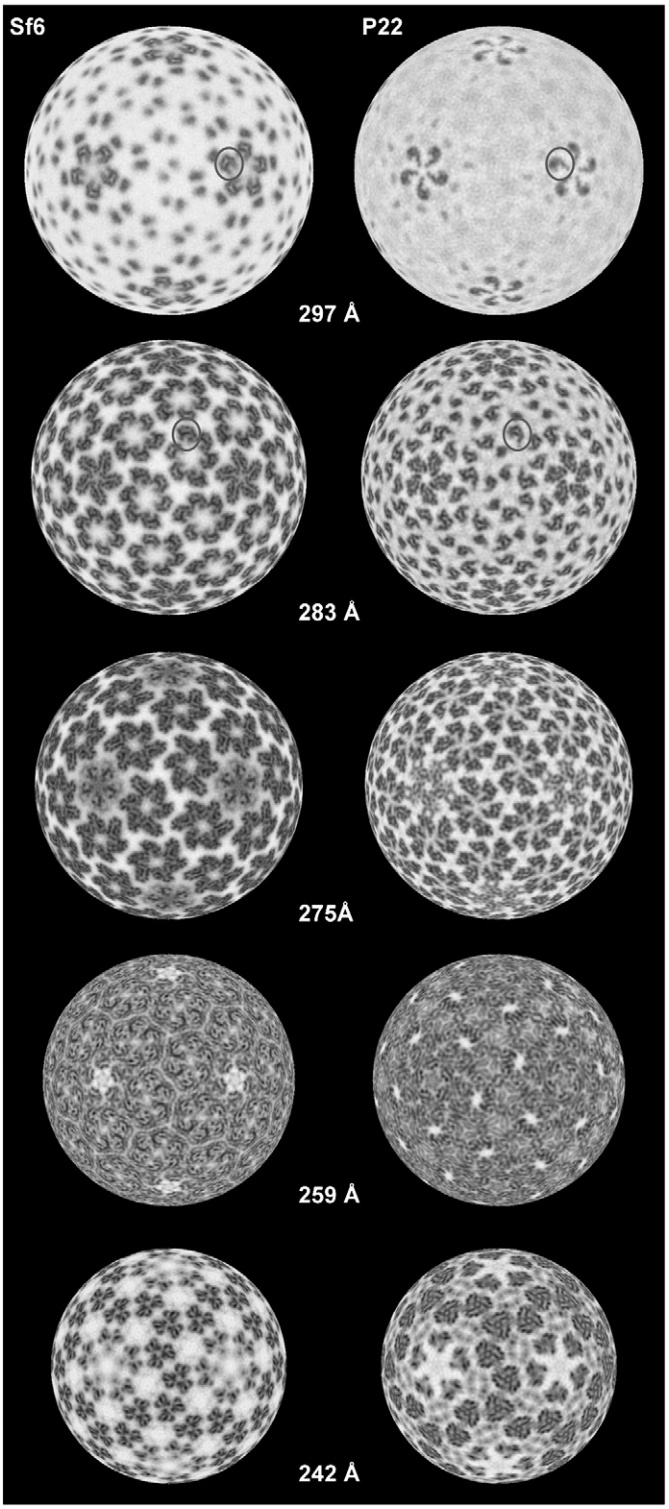

Fig. 3. Radial density projections of Sf6 and P22 procapsids. Projected density distributions at different radii illustrate similarities and differences in the tertiary and quaternary structures of the two procapsids. Each projection shows the density contained within a spherical ~1-Å thick annulus. Individual telokin domains are highlighted (black circles) in Sf6 and P22 in a penton (r = 297 Å) and in a hexon (r = 283 Å).

reconstruction can be assigned with confidence to the scaffolding protein (gp4; 33.5 kDa). This likely indicates that the scaffold is not organized with the icosahedral symmetry that was imposed during the reconstruction process. This is also true of P22 procapsids; however, a recent 3.8 Å resolution P22 procapsid density map suggested that a "V-shaped" volume of density represents the C-terminal 65 residues of the P22 scaffolding protein (gp8; 33.6 kDa) (Chen et al., 2011; Sun et al., 2000). More thorough biochemical analysis will be needed to confirm the precise identity of this density in Sf6.

Secondary structure predictions for the CPs of Sf6 and P22, as determined with PSIPRED (McGuffin et al., 2000) (GenBank accession Nos. Sf6, AF547987; P22, BK000583), support the notion that the two subunits are quite similar despite being only ~14% identical in sequence (Fig. 4). We also analyzed the sequence of the Sf6 CP using FFAS03, a fold and function assignment system used to identify and quantify homology between proteins with ~30% or less sequence identity (Jaroszewski et al., 2005). The top match for the Sf6 CP was a pseudo-atomic model of the P22 CP (PDB ID 3IYH) (Parent et al., 2010a) (Table 3). Additional hits with lower, albeit reliable, scores included the CPs of other dsDNA bacteriophages that share HK97-like structural elements as well as the human FC gamma receptor, which has an Ig-like fold similar to telokin (Table 3). Despite these predicted similarities between Sf6 and P22, detailed homology modeling of the Sf6 CP proved to be problematic. First, two models of the P22 CP have been reported that differ primarily in the interpretation of the C-terminal ~130 residues (Chen et al., 2011; Parent et al., 2010a). Second, there is no reliable way to constrain or confirm the modeling process given the current paucity of biochemical and biophysical data for the Sf6 CP.

Despite the high conservation of secondary structural elements in the P22 and Sf6 CPs, the two procapsids exhibit clear differences in tertiary and quaternary structures, which must be dictated by the large differences in the amino acid sequences. Indeed, the two proteins have very different isoelectric points (pI) of 6.09 and 4.97 for Sf6 and P22, respectively, as determined by the ProtParam server (Gasteiger et al., 2005). Such differences are consistent with the slower mobilities of Sf6 procapsids and virions compared to P22 in agarose gels, which reflect the surface charge differences between particles with very similar sizes and masses (described below).

Icosahedral 3D reconstruction of Sf6 virion

An icosahedrally-averaged, 3D cryo-reconstruction of the Sf6 virion was computed from 15,483 particle images, yielding a density map of the mature Sf6 head structure at an estimated resolution of 7.0 Å (Table 2; Materials and methods). As was also true for the procapsid, the overall morphologies of the mature Sf6 and P22 heads are similar but they differ in detail. The dsDNA genome is tightly packed inside the Sf6 capsid within a series of discrete, concentric shells (at least six are visible in Fig. 5A). Dense packing of the genome is found in P22 and other tailed dsDNA phages and herpesviruses (Johnson and Chiu, 2007). The Sf6 CP appears to contact the outermost shell of the genome (Fig. 5A) in a manner similar to that seen in bacteriophage ϕ29 (Tang et al., 2008), but in P22 the CP does not appear to directly contact the genome. Though CP–DNA interactions in Sf6 and ϕ29 may help stabilize the highly condensed genome, additional experimental evidence is needed to verify this hypothesis and to explain why P22 appears to lack such interactions.

Differences between the structures of the procapsid and phage head provide one means to explore the process by which the CP shell matures (expands) when procapsids convert into virions. Maturation in the well-studied HK97 system involves dramatic movements of the spine helix and N-arm, which lead to considerable thinning and increased stability of the capsid shell (Gertsman et al., 2009). P22 maturation includes conformational changes similar to those of HK97, and also movements of the A-domain close off the axial holes present in the procapsid capsomers (Teschke and Parent, 2010). In Sf6, maturation also involves wall thinning and shell expansion (Sf6 virions have an ~90 Å larger maximum diameter than procapsids). The axial holes of the Sf6 hexons become occluded in virions (Fig. 5B), whereas the pentons are occluded prior to

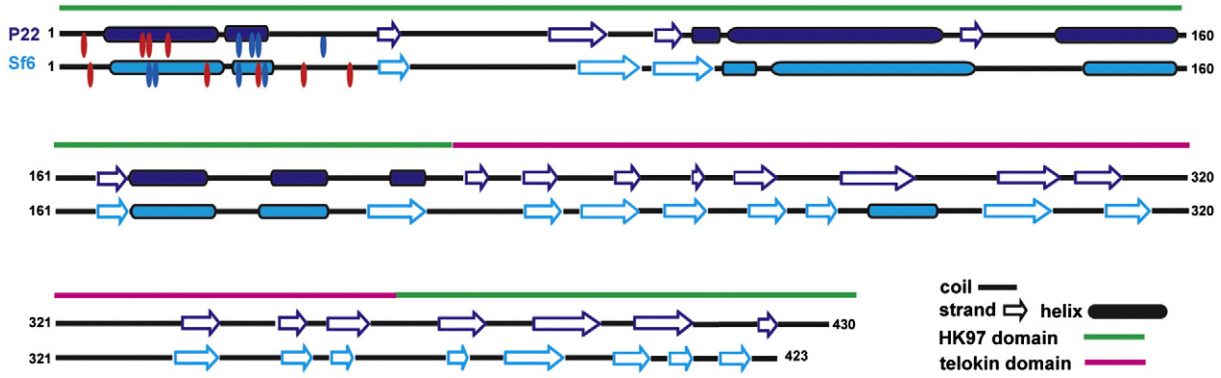

Fig. 4. Secondary structure predictions for the CPs of Sf6 and P22. The PSIPRED server (McGuffin et al., 2000) was used to predict the secondary structures of the CPs of Sf6 and P22. Regions of the CPs that correspond to predicted helices and β-strands are depicted as cylinders and arrows, respectively. Regions that correspond to the HK97-like fold and the telokin domain, as defined by a pseudo-atomic model of P22 (Parent et al., 2010a), are shown as green and magenta lines, respectively. Charged residues in the N-arm are marked by ovals (red for acidic and blue for basic).

maturation (above; Fig. 1E). The spine helix and putative N-arm in the Sf6 CP rearrange during maturation (data not shown), and movements of these structural elements are similar to those observed during P22 maturation (Parent et al., 2010a). In P22, the N-arm domain of CP has been suggested to provide a binding site for scaffolding protein, and its conformation switches during dsDNA packaging, likely triggering release of the scaffolding proteins (Chen et al., 2011; Parent et al., 2010a). In spite of large differences in sequence, the highly charged CP N-termini and scaffolding protein C-termini in P22 and Sf6 suggest that the N-arm in the Sf6 CP functions similarly in assembly and maturation.

Asymmetric cryo-EM reconstruction of the Sf6 virion

The structure of the Sf6 virion was also reconstructed without imposing any symmetry during the image processing (Fig. 6A). This asymmetric reconstruction, computed from 16,253 particle images and reaching an estimated 16-Å resolution (Table 2), includes reliable structural details for the dodecameric portal complex (gp3) and the tail machine, which contains twelve gp7 and six gp8 subunits, six tailspikes (each a trimer of gp14), and the tail needle (trimer of gp9). A central density section of the Sf6 virion shows the organization of many virion components (Fig. 6B). These include the CP shell (415 copies of gp5), the concentric layers of densely packed dsDNA genome, the portal complex at the unique vertex at the junction between capsid and tail, and the tail machine. We docked the crystal structure of the receptor-binding domain of one Sf6 tailspike trimer (PDB ID 2VBK (Muller et al., 2008)) as a rigid body into the density map. In addition, we also fit the known structures of Sf6 orthologs from phage P22 (Fig. 6C). These included the crystal structures of the complete dodecameric portal complex (PDB ID 3LJ4 (Olia et al., 2011)), a trimeric tail needle homology model (seen in Fig. 5B of (Bhardwaj et al., 2011) that includes the crystal structure of the Sf6 tail needle (gp9) knob (PDB ID 3JR0)), the P22 gp4 tail protein (PDB ID 1VT0 (Olia et al., 2011)), and the segmented density of the P22 gp10 tail protein (EMDB ID 5051) extracted from a cryo-

Table 3
FFAS03 results.

Score	PDB ID	Protein	# residues
−101	3IYH (Parent et al., 2010a)	P22 CP	430
−45	2XVR (Ionel et al., 2011)	Phage T7 CP	345
−42	2XD8 (Liu et al., 2010)	Cyanophage P-SSP7 CP	375
−6	1OHG (Wikoff et al., 1999)	HK97 CP (mature state)	282
−6	3E8K (Gertsman et al., 2009)	HK97 CP (prohead II state)	273
−4	1E4J (Sondermann et al., 2000)	Human FC gamma receptor	176

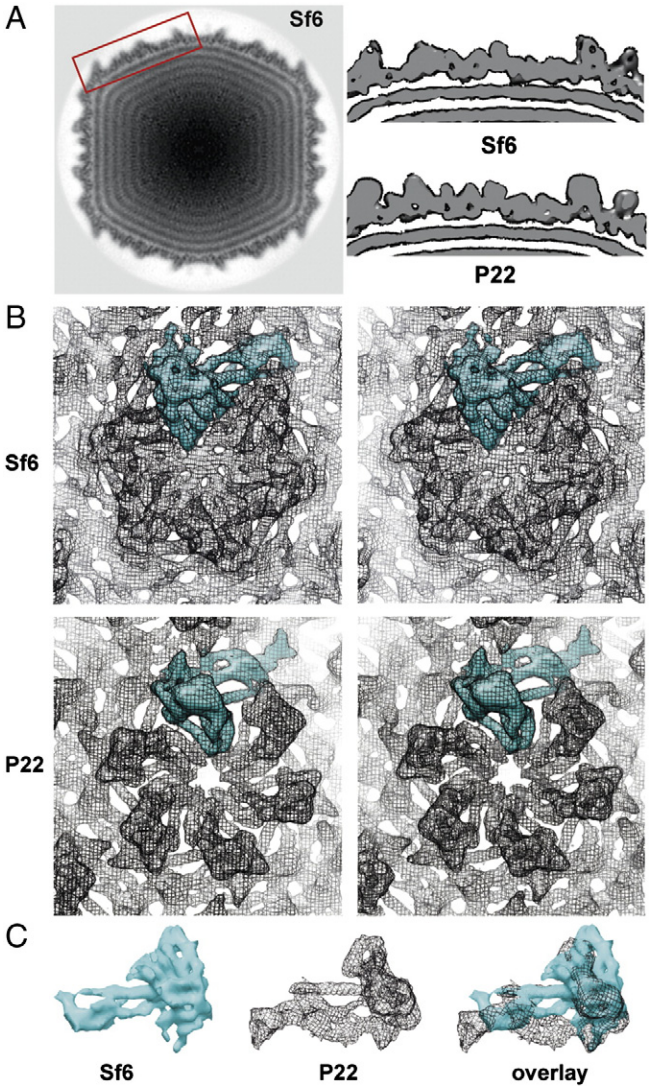

Fig. 5. Comparisons of icosahedrally-averaged capsids of Sf6 and P22 virions. A. Equatorial density section from the Sf6 virion cryo-reconstruction, with features of highest and lowest density depicted in black and white, respectively. Rectangular box outlines the region of Sf6 shown as a surface-rendered slab at top right. The corresponding region of P22 is shown at the bottom right. B. Stereo views of hexons with a CP monomer in each view shown in cyan, highlight notable differences in the tertiary structures of the CPs in Sf6 and P22. C. Segmented density envelopes of individual CPs from Sf6 (cyan, solid density) and P22 (black mesh), and the two aligned with respect to the spine helices and superimposed using Chimera (Goddard et al., 2007).

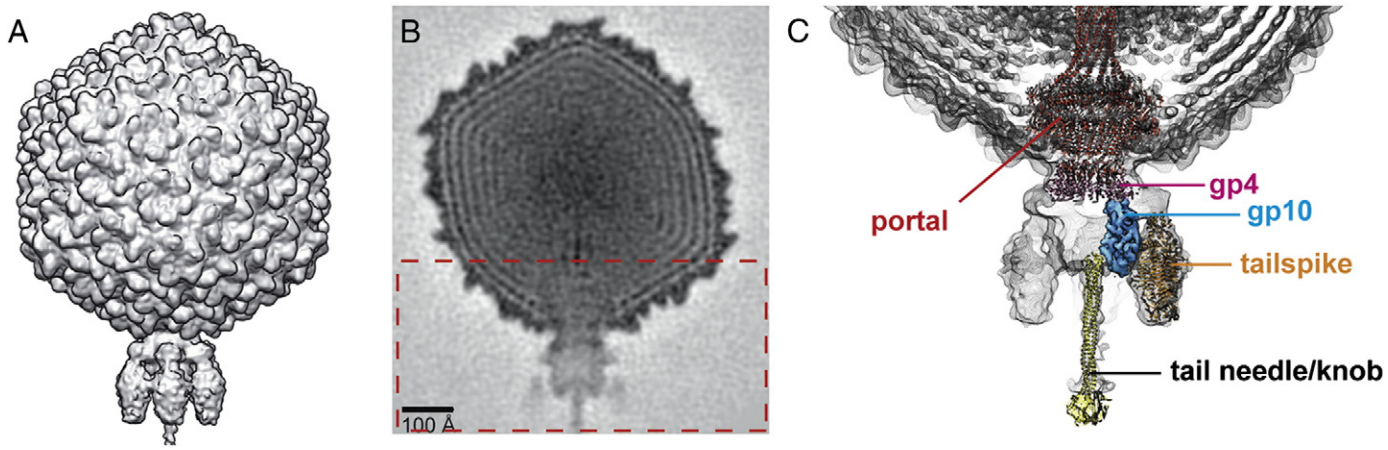

Fig. 6. Sf6 virion structure. A. Shaded-surface representation of the Sf6 virion, reconstructed by asymmetric methods to an estimated resolution of 16 Å. B. Equatorial, cross-section (1 pixel, or ~2.1 Å thick) from the Sf6 virion density map shown in A, with highest and lowest density features depicted in black and white, respectively. The rectangular box outlines the region of the virion map enlarged in C. C. Sf6 virion density map (gray mesh) plus the fitted crystal structures of the Sf6 tailspike (orange; PDB ID 2VBK), the P22 gp1 portal (red; PDB ID 3LJ4), the P22 gp4 tail protein (pink; PDB ID 1VT0), the Sf6 tail needle homology model, and the segmented density for the P22 gp10 tail protein (blue; EMDB ID 505) extracted from the tail machine cryo-reconstruction of Lander et al. (2009).

reconstruction of the isolated P22 tail machine (Lander et al., 2009). All of these virion components, which are similar in size in Sf6 and P22 (Table 1), were fit without remodeling into the Sf6 density map. Hence, the Sf6 and P22 virions have quite similar structures overall. The Sf6 portal structure closely mimics that observed in P22 virions, and includes the long barrel domain that was hypothesized to be present in many other tailed phages (Olia et al., 2011; Tang et al., 2011). The central channel of the barrel domain appears to contain a linear stretch of DNA. In Sf6, the barrel is at least 80% the height of the P22 barrel, but, at the current resolution of our virion cryo-reconstruction, we cannot unambiguously determine the full extent of the Sf6 barrel because this portion is masked by what appears to be disordered genome density near the center of the phage head. Finally, as remains true for P22, we were unable to locate density in the virion reconstruction that could be assigned unambiguously to any of the three ejection proteins.

OmpA and OmpC are not components of Sf6 procapsids or virions

Recently, an ~20-Å resolution, icosahedrally-averaged cryo-reconstruction of the Sf6 virion was determined in which density features adjacent to the inner surface of the CP shell were interpreted as arising from *S. flexneri*, host-encoded, major outer membrane proteins OmpA and OmpC (36 and 32 molecules, respectively) (Zhao et al., 2011). This interpretation was based on two observations. First, OmpA and OmpC were identified by SDS-PAGE and mass spectrometry in preparations of Sf6 phage particles that had been purified through CsCl step gradients. Second, an Sf6 minus P22 virion density difference map showed the presence of positive difference density. OmpA and OmpC were also present in our preparations of virions that were purified on a CsCl step gradient from Sf6-infected *Shigella*. N-terminal sequencing and mass spectrometric analyses of these proteins (the two SDS-PAGE bands labeled "?" in part A of Fig. 2 of Casjens et al., 2004) confirmed that they were OmpA and OmpC. However, we found no evidence for the putative Omp protein density in any of the three Sf6 cryo-reconstructions presented here. We do not see any features in the 3D density maps that correspond to a β-barrel in the positions reported by Zhao et al. (2011) (β-barrel structural elements are common to OmpA and OmpC; PDB IDs 1QJP and 2J1N (Basle et al., 2006; Pautsch and Schulz, 2000)). When we calculate an Sf6 minus P22 difference density map similarly to Zhao et al. (2011), but using our 7 Å resolution data, we do see positive difference density in the same places as they observed. However, the higher-resolution achieved in our structures, combined with prior knowledge of the P22 CP fold (Parent et al., 2010b) allows us to define the molecular envelope of the Sf6 CP, and it appears that the observed differences result from quaternary structural differences between Sf6 and P22 (discussed above).

To unequivocally determine if OmpA and/or OmpC are components of Sf6, we used native agarose gel electrophoresis to separate the Sf6 procapsid and virion products from phage infected cells (see Materials and methods). The gels showed two distinct bands and a significant amount of material that remained in the well (Fig. 7A).

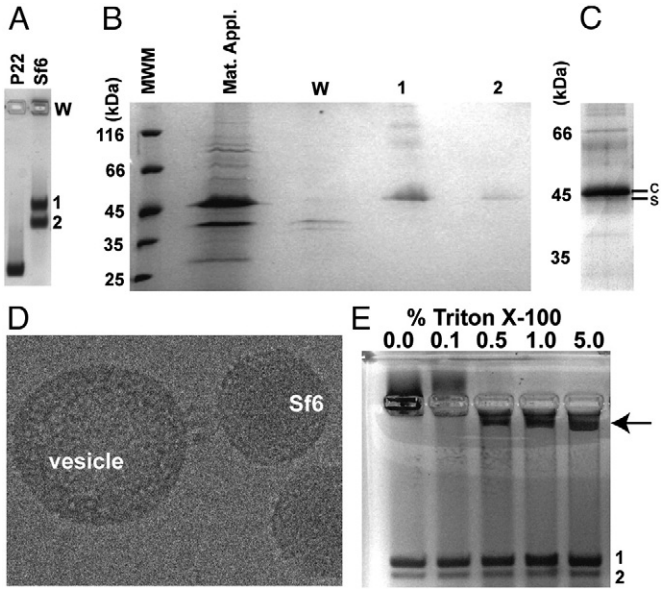

Fig. 7. Omps A and C are not associated with assembled particles. A. Coomassie-stained agarose gel showing P22 procapsids as a control (left lane) and assembly products from an Sf6 infection (right lane). B. SDS gel of the Sf6 sample shown in panel A, stained with Coomassie (W = well; MWM = molecular weight marker). C. Silver-stained SDS gel of material extracted from band 2 (from gel shown in A), enlarged to emphasize the separation between the scaffolding protein ("s") and CP bands ("c"). D. Cryo-electron micrograph of a representative Sf6 virion that appears to be docked to a lipid vesicle that co-purified with virions in a CsCl gradient. E. Coomassie-stained agarose gel of Sf6 virions from a Triton X-100 titration. Increasing amounts of the material associated with the well in the first lane (marked "0%") enter the gel as the detergent concentration increases (arrow points to this material in lane 5).

As determined by ethidium bromide staining, the slower migrating band (band 1) contained dsDNA and the faster migrating band (band 2) did not (data not shown). We used SDS-PAGE and mass spectrometry to identify proteins in each band and in the well (Materials and methods). Bands 1 and 2 and the well were excised from the agarose gel, and the proteins were TCA-precipitated and visualized by SDS-PAGE (Fig. 7B). The major components in the wells corresponded to OmpA and OmpC and Sf6 phage proteins were minor components. Band 1 contained all of the expected Sf6 virion proteins. Although Coomassie staining only revealed CP in band 2 (Fig. 7B), silver staining revealed the presence of all expected procapsid proteins (Fig. 7C). The Sf6 scaffolding protein migrates very near to CP in SDS-PAGE (Fig. 7C) despite substantial differences in their predicted molecular masses (Table 1). Slower than expected mobility has been reported for scaffolding proteins in phages T7 (Cerritelli and Studier, 1996) and Syn5 (Raytcheva et al., 2011), and this was attributed to the large number of charged residues, extended conformations, and low theoretical pIs (4.3 and 4.1, respectively, for T7 and Syn5). The theoretical pI of the Sf6 scaffolding protein is 4.6, which may explain its SDS-PAGE mobility. Several different types of purification and separation procedures were performed (CsCl purified, $CHCl_3$ extracted, size exclusion chromatography (SEC) purified +/− detergent, and sucrose gradient purified), and in all instances OmpA and OmpC remained in the wells after agarose electrophoresis of the particles. Finally, we constructed mutant *S. flexneri* strains that lack either the *ompA* or *ompC* gene (see Materials and methods). Sf6 propagates in both of these mutant hosts, and OmpA or OmpC is missing from virion preparations grown in *ompA*- or *ompC*-hosts, respectively (data not shown). All the above findings demonstrate quite convincingly that neither protein is required for Sf6 virion formation and neither is present in Sf6 virions. However, the source of these proteins and the reason why they co-purify with Sf6 particles remained unknown.

Sf6 virions from *Shigella* lysates show, even after CsCl step gradient purification, a few percent of particles with their tails apparently attached to host-derived membrane vesicles (Fig. 7D). P22 particles prepared from *Salmonella* lysates (as well as several other P22-like phages) do not show such attached vesicles (data not shown). We hypothesize that OmpA and OmpC present in the vesicles in the *Shigella* lysate accounts for them being contaminants in the purified phage samples. To test this idea further, we treated the Sf6 samples with increasing amounts of Triton X-100 and examined the products by agarose gel electrophoresis and mass spectrometry. At levels of Triton X-100 exceeding 0.1%, conditions under which Sf6 virions remain intact, material retained in the agarose gel wells decreased, and a new, slower-migrating band appeared (arrow in Fig. 7E). Mass spectrometry analysis of this band revealed that it contained several *S. flexneri*, membrane-associated proteins, with the major components being OmpA and OmpC. We conclude that detergent liberates OmpA and OmpC from the lipid vesicles that co-purify with Sf6 virions, and that the material trapped in the wells of the agarose gels (Figs. 7A and E) represents the virion-vesicle complexes seen by cryoEM.

Sf6 is slightly less stable than P22

Products obtained after heat-treatment of P22 virions and procapsids have been examined by agarose gel electrophoresis to monitor the thermal-induced changes in these particles (Parent et al., 2010b). We performed heating and electrophoresis experiments with procapsids and virions of Sf6 and P22 to compare their stabilities. The results showed that Sf6 procapsids and virions are slightly less stable than their P22 counterparts (Fig. 8A). As previously reported and reproduced here, heat treatment causes P22 procapsids to swell and transform into “expanded heads” (ExH), which are particles that lack scaffolding protein and pentons but have expanded (Parent et al., 2010a; Teschke et al., 2003). No band corresponding to expanded heads was found in heat-treated Sf6 samples, and negative stain transmission electron microscopy confirmed that heated P22 samples contained ExH particles but heated Sf6 samples did not (data not shown).

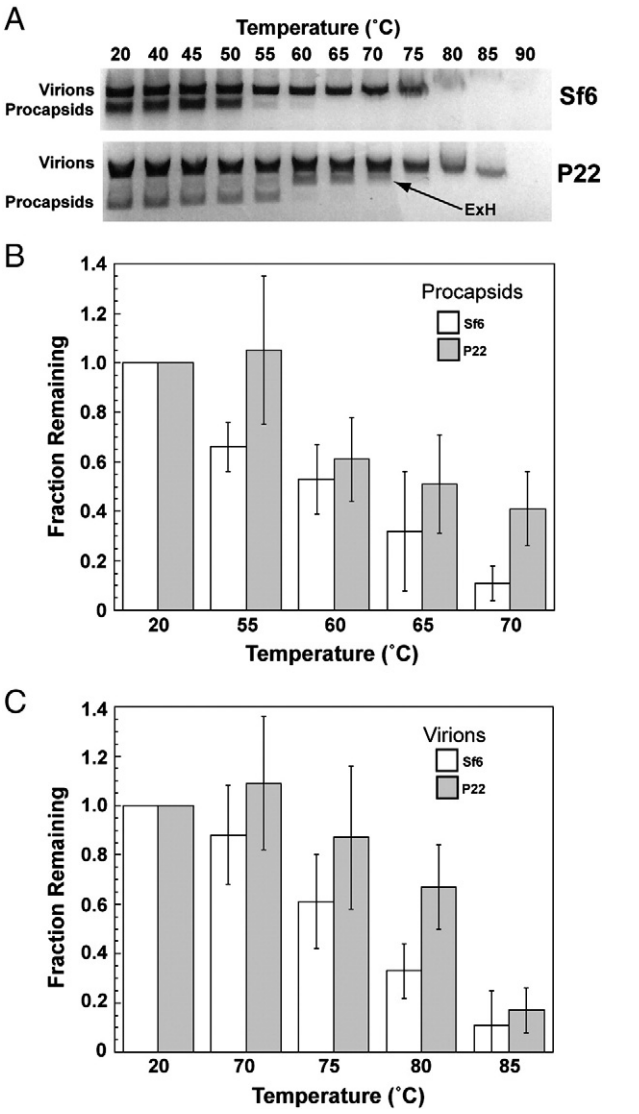

Fig. 8. Relative stabilities of Sf6 and P22. A. Agarose gel of phage assembly products treated at different temperatures for 15 min. The expanded, penton-less heads (“ExH”) in P22 (arrow) appear as a major component of the heat-treated sample. Quantification of the fraction of intact procapsid (B) and virions (C) remaining after heat treatment (data shown only for select temperatures). These data are an average from three independent experiments (error bars denote the standard deviation of the measurements).

Discussion

Sf6 CP has an HK97-like core and a telokin domain

The CPs of all tailed bacteriophages (*Myoviridae*, *Siphoviridae*, *Podoviridae*) and some large dsDNA eukaryotic viruses (*Herpesviridae*) share a common fold (Bamford et al., 2005). It is not surprising therefore, that our cryo-reconstructions of Sf6 reveal a CP protein with an “HK97-like” core. However, like P22 but unlike other known virion structures, the Sf6 CP includes a surface-exposed, Ig-like, “telokin” domain (Parent et al., 2010a). The presence of this domain suggests that it is likely a conserved feature specific to the P22-like phages.

The twelve essential genes that encode the P22-like virion proteins show substantial variation within this phage group, and P22 and Sf6 represent two quite different members of this group (Casjens and Thuman-Commike, 2011). The virion assembly proteins of the two phages range from having 93% identity in a.a. sequence (tail protein gp10) to having no recognizable similarity (e.g., small terminase subunit, scaffolding protein, and receptor-binding domain of the tailspike). Distantly related species of tailed phages are proposed to have undergone "rampant" horizontal transfer of virion assembly genes during their evolution (Casjens, 2005; Hendrix, 2002). Thus, it is not clear whether the differences between orthologous P22 and Sf6 virion assembly genes arose through divergence within the larger P22-like phage group or whether the differences arose by horizontal transfer of genetic material into the P22-like group from other phages. The Sf6 and P22 CPs (only 14% identical) are among those viral proteins whose evolutionary history is uncertain. The results presented here show that, unlike the CPs of other tailed phages, the Sf6 CP contains a telokin-like domain that is very similar to that of P22, and this supports the idea that the CP has diverged *within* the P22-like group rather than from horizontal exchange with other phage types. This, however, does not mean that horizontal exchange cannot occur between the P22-like and other phage groups. Indeed, evidence suggests that the tailspike and small terminase subunit genes have exchanged with other phage types (Casjens and Thuman-Commike, 2011). Nonetheless, the P22-like phage group appears to be very ancient, with CP variants (and probably most other virion assembly proteins) having diverged within this group to the point of losing or nearly losing recognizable sequence similarity. The P22-like portal proteins, scaffolding proteins, CPs, and the gp4 tail adaptor proteins all have very similar phylogenetic trees, which suggests that these procapsid assembly proteins have co-evolved without import of outside genetic information, and thus that they all diverged in parallel within the P22-like phage group (Casjens and Thuman-Commike, 2011).

Capsids are stabilized by CP contacts at sites of three-fold symmetry

In spite of having CPs with similar folds, capsid assembly and the subsequent stabilization that accompanies maturation in dsDNA-containing phages and in HSV-1 can occur by several different mechanisms. For example, HK97 utilizes a covalent crosslinking mechanism (Wikoff et al., 2000) that forms "molecular staples" via P-loops at all three-fold sites during maturation (Gertsman et al., 2009). HK97 also includes a key, intercapsomeric salt bridge at this position, where residue substitutions reduce particle stability or eliminate capsomer assembly (Gertsman et al., 2010). The presence of auxiliary "decoration" or "cement" proteins in other phages and viruses provides another common mechanism for stabilizing virions at three-fold and quasi-three-fold positions. Examples include gpD of λ (Lander et al., 2008; Sternberg and Weisberg, 1977; Yang et al., 2008), Dec of phage L (Gilcrease et al., 2005; Tang et al., 2006), gpE of ε15 (Jiang et al., 2008), and the triplexes of HSV-1 (Brown and Newcomb, 2011). Recently, a pseudo-atomic model of the P22 CP indicated that capsid stabilization in P22, which has no auxiliary protein and does not employ cross-links, may also occur through strong interactions between neighboring capsomers at the strict and quasi three-fold symmetry axes via the P-loops (Parent et al., 2010a). The recent cryo-reconstructions of phage 80α procapsids and virions, which show CPs form "trefoil" structures at both types of three-fold sites (Spilman et al., 2011), further support the notion that strong stabilizing interactions commonly occur at these locations. Like P22, Sf6 CP does not form chemical crosslinks and the Sf6 genome does not encode any auxiliary decoration protein (Casjens et al., 2004). In addition, our cryo-reconstruction of Sf6 procapsids reveals that the most extensive CP:CP contacts reside at the three-fold sites, which suggests that this feature is conserved among dsDNA-containing phages.

Capsomer maturation and A-domain flexibility

An obvious distinction between the Sf6 and P22 structures is the presence or absence of structural elements near the centers of the capsomers. In the Sf6 procapsid, hexons have small central holes and the pentons are closed. This contrasts with the P22 procapsid, where the hexons and pentons both contain central holes that are larger than those in the Sf6 hexons. Variations in the P22 CP at position 170 that increase rigidity of the A-domain result in procapsids with closed pentons (Suhanovsky et al., 2010). CP variants that resulted in increased A-domain rigidity also led to a lower energy barrier to procapsid maturation and an increase in the appearance of aberrant assembly products such as polyheads (Parent et al., 2010b). It may be that the A-domain in Sf6 is inherently more rigid than in other P22-like phages, and this favors the closed state of capsomers in procapsids. However, there does not seem to be a corresponding change in thermal stability between Sf6 and P22 procapsids, nor did we observe any aberrant assembly products in our studies. Perhaps the flexibility of the A-domain does not play the same role in regulating maturation of the Sf6-like subgroup of phages.

Cell recognition and attachment in Podoviridae

For members of the family *Podoviridae*, the tailspike proteins are the primary viral components that function in cell-recognition and attachment. Crystal structures have been determined for the P22 and Sf6 tailspike proteins, and the endorhamnosidase activity of both of these proteins has been thoroughly documented (Muller et al., 2008; Steinbacher et al., 1994). It has been postulated that a secondary receptor might be required to trigger DNA release from the virion (Casjens and Molineux, 2012; Chang et al., 2010). However, for P22, the lipopolysaccharide of the host is sufficient to allow genome release, albeit slowly, in vitro (Andres et al., 2010), and this indicates that a secondary membrane protein receptor may not be needed for P22 to infect *Salmonella*.

The observation of host membrane vesicles stably bound to Sf6 virion tails is nonetheless provocative, since the tailspike endorhamnosidase might remove all of the O-antigen polysaccharide, thereby leaving nothing to which the tailspike could bind. This raises the question of whether the Omp proteins or perhaps a different secondary receptor, are involved in binding. OmpA is a major component of the outer membranes of enterobacteria, with ~100,000 copies present on the surface of each bacterium (Koebnik et al., 2000). In *Escherichia coli*, OmpA is a transmembrane protein, and surface-exposed loops that connect the transmembrane domains act as the site for host recognition and attachment for a number of coliphages (Morona et al., 1984). OmpC has also been implicated as a cell surface receptor for bacteriophages (Ho and Slauch, 2001; Tanji et al., 2008; Yu and Mizushima, 1982). The OmpA and OmpC proteins are both virtually identical in *E. coli* and *S. flexneri* and could be universally present, cell recognition sites for P22-like phage. Our results reveal that neither of these Omp proteins is associated with the Sf6 capsid, but instead both associate with the lipid vesicles that co-purify with virions. This phenomenon has yet to be reported for any other P22-like phage. The recently determined crystal structure of the Sf6 tail needle-knob shows significant conservation with the structures of the cell receptor binding motifs in PRD-1 phage and adenovirus (Bhardwaj et al., 2011). This suggests that the knob of the tail needle may promote lipid vesicle co-purification with Sf6 and could be driven in part owing to the high concentrations of OmpA and OmpC in our samples. The fact that Sf6 infects OmpA- and OmpC-knockouts shows that neither of these proteins is absolutely required for infection; however, they could still serve an auxiliary function or they could be involved if they have redundant function with regard to Sf6 binding. Alternatively, Sf6 may not bind to *S. flexneri* via a secondary receptor, but rather through the tailspikes or even through non-

specific hydrophobic interactions with the lipid vesicles, and could mean that OmpA and OmpC are simply contaminant "cargo".

Roles of the D-loops and telokin domains in P22-like phages

The CPs of Sf6 and P22, despite having quite distinct sequences, exhibit a strikingly similar pattern of secondary structure elements (Fig. 4). The folds of these CPs are similar overall, but differ in a few key ways. A recent, higher-resolution cryo-reconstruction study of P22 procapsids indicates that capsid stability in P22 may arise not only from interactions among P-loops at the three-fold sites, but also from inter-subunit D-loop interactions between capsomers (Chen et al., 2011). The Sf6 procapsid has no obvious D-loop structure, and neighboring capsomers only minimally contact each other, indicating that Sf6 lacks a P22-like D-loop function. Whether P22 gained or Sf6 lost D-loop function during evolution remains an open question. Nonetheless, Sf6 procapsids function without the D-loop, and they are only slightly less heat stable than P22.

In P22, the telokin domains do not contact one another and each domain is only associated with a single CP monomer (Parent et al., 2010a). Hence, these domains are not responsible for stabilizing P22 particles by bridging to adjacent subunits. Instead, the domain appears to function primarily as a folding nucleus for the HK97-like core structure (Teschke and Parent, 2010). However, in striking contrast, the telokin-like domain in Sf6 makes extensive intra-hexon contacts between subunits (Fig. 2, r = 275 Å). These contacts may enhance capsomer stability and/or they may confer some advantage during assembly of CPs that lack D-loop structures.

Materials and methods

Preparation and purification of Sf6 virions and procapsids

Luria Broth (LB) was used to support bacterial growth for the preparation of phage and procapsids. *S. flexneri* strain PE577 (Morona et al., 1994) was grown in LB at 37 °C to 1×10^8 cells/mL. Phage Sf6 (clear plaque mutant (Casjens et al., 2004)) infection was initiated at a multiplicity of infection of 0.1. The culture was shaken until near-complete lysis occurred (~3.5 h at 37 °C). Chloroform was added to ensure complete lysis, and cell debris was removed by centrifugation (Sorvall SS-34 rotor, for 10 min at 10,000 rpm, 4 °C). Phage and procapsids were then concentrated at 18,000 rpm for 90 min at 4 °C. The resulting pellet was resuspended by nutation at 4 °C overnight, in M9 salts supplemented with 2 mM $MgSO_4$. Aggregated material was removed by centrifugation and the phage/procapsid preparation was stored at 4 °C. Further purification using a CsCl step gradient was performed as described (Casjens et al., 2004).

Cryo-transmission electron microscopy

Small (3.5 μL) aliquots of purified phage and procapsids (at ~1×10^{14} phage/mL or ~10 mg/mL) were vitrified and examined using established procedures (Baker et al., 1999). Samples were applied to holey Quantifoil grids that had been glow-discharged for ~15 s in an Emitech K350 evaporation unit. Grids were then blotted with Whatman filter paper for ~5 s, plunged into liquid ethane, and transferred into a precooled, FEI Polara, multi-specimen holder, which maintained the specimen at liquid nitrogen temperature. Micrographs were recorded on Kodak SO-163 electron-image film in an FEI Polara microscope operated at 200 keV and under minimal-dose conditions (~22 e/Å^2) at a nominal magnification of 59,000×. Additional data collection statistics, including the range of objective lens defocus settings used to record each set of micrographs, are listed in Table 2. The programs RobEM (http://cryoEM.ucsd.edu/programs.shtm) and ctffind3 (Mindell and Grigorieff, 2003) were used to extract individual particles and estimate the level of defocus and astigmatism for each micrograph.

Icosahedral cryo-reconstructions of Sf6 procapsid and virion

Image processing for each of the two separate data sets (procapsids and virions) was performed in the same manner as follows. Micrographs that exhibited minimal astigmatism and specimen drift were selected for further processing and digitized at 6.35 μm intervals (represents 1.07 Å per pixel) on a Nikon Super Coolscan 8000, and image preprocessing was performed as described (Baker et al., 1999). A subset of 150 particle images was used as input to the random-model computation procedure to generate an initial 3D density map at ~25 Å resolution (Yan et al., 2007a). This map was then used to initiate determination and refinement of particle orientations and origins for the complete set of images using version 4.01.07 of AUTO3DEM (Yan et al., 2007b). Phases and amplitudes of the particle structure factor data were corrected to compensate for the effects caused by the microscope contrast-transfer function (Bowman et al., 2002). The Fourier Shell Correlation criterion ($FSC_{0.5}$) was used to estimate the resolution of each reconstruction (Table 2) (van Heel and Schatz, 2005). Graphical representations were generated with the RobEM and Chimera (Goddard et al., 2007) visualization software packages.

Asymmetric cryo-reconstruction of Sf6 virion

The general strategy we used to process the Sf6 virion images and compute an asymmetric reconstruction was similar to that used to derive an asymmetric reconstruction of the P22 virion (Lander et al., 2006). First, all digitized micrographs of the Sf6 virion samples were binned 2X, which generated a pixel size of 2.14 Å. Then, we re-boxed all virion images within a box window that was large enough to assure that the tail of each particle was not excluded as was the case during the icosahedral processing strategy described above. Also, the origin and orientation parameters of each virion image were set to match those determined during the icosahedral processing. Next, we used the "ticos_equiv" option in AUTO3DEM (v4.01.07) (Yan et al., 2007b) to determine an initial estimate of the orientation that properly aligns the tail in each virion image to a common reference, which was the 17-Å resolution 3D cryo-reconstruction of P22 (EMDB ID 1220 (Lander et al., 2006)). Next, iterative refinement of the origin and orientation of each virion image was performed in AUTO3DEM set to operate in "asymmetric" mode, in which no symmetry is assumed or imposed on any of the data. It is important to note that the P22 reconstruction did not introduce any model bias into the Sf6 asymmetric reconstruction process. This was clearly evident because the final Sf6 reconstruction showed a head structure with all of the features that distinguish Sf6 from P22. In addition, the final Sf6 reconstruction showed a tail structure that was similar overall, yet distinct in detail from the P22 tail. Finally, the tip of the tail needle is partially missing in the Sf6 cryo-reconstruction (Fig. 5) because the size of the box window was reduced slightly to keep computations efficient and within memory limits and to reduce unwanted background noise.

Agarose and polyacrylamide electrophoresis gels

Samples (~1 mg/mL) were diluted with ice-cold agarose sample buffer (0.25% bromophenol blue and 10% glycerol in TAE buffer: 40 mM Tris acetate and 1 mM EDTA). Approximately 10 μg of protein was loaded in each lane of a 1.0% Fisher agarose gel (modified from Serwer and Pichler, 1978). The gel was run at 110 V for 120 min at room temperature and stained with Coomassie blue. Bands were excised with a razor blade, and the agarose was solubilized in 500 μL QB buffer from a Qiagen gel-extraction kit at 50 °C for 10 min. The total protein in each sample was either 1) TCA precipitated, visualized

by SDS-PAGE (10% gel), and either Coomassie stained (wells and virion band) or silver-stained (procapsid band) using a SilverQuest staining kit (INVITROGEN) or 2) analyzed by mass spectrometry as described below.

In-gel digest for mass spectrometry

Samples were dried in a speedvac, reduced with 200 μL of 100 mM ammonium bicarbonate-10 mM DTT and incubated at 56 °C for 30 min. The liquid was removed and 200 mL of 100 mM ammonium bicarbonate 55 mM iodoacetamide was added to the gel pieces and incubated at room temperature in the dark for 20 min. After the removal of the supernatant and one wash with 100 mM ammonium bicarbonate for 15 min, the same volume of acetonitrile (ACN) was added to dehydrate the gel pieces. The solution was then removed and samples were dried in a speedvac. For digestion, enough solution of ice-cold trypsin (0.01 μg/mL) in 50 mM ammonium bicarbonate was added to cover the gel pieces and set on ice for 30 min. After complete rehydration of the pieces, excess trypsin solution was removed and replaced with fresh 50 mM ammonium bicarbonate and then incubated overnight at 37 °C. The peptides were extracted twice by the addition of 50 μL of 0.2% formic acid and 5% ACN and vortexed at room temperature for 30 min. The supernatant was removed and saved. A total of 50 μL of 50% ACN-0.2% formic acid was added to the sample, which was vortexed again at room temperature for 30 min. The supernatant was removed and combined with the supernatant from the first extraction. The combined extractions were analyzed directly by LC in combination with tandem mass spectroscopy (MS/MS) using electrospray ionization.

LC–MS/MS analysis

Trypsin-digested peptides extracted from SDS-PAGE as described above were analyzed by liquid chromatography (LC)–MS/MS with electrospray ionization. All nanospray ionization experiments were performed with a QSTAR-Elite hybrid mass spectrometer (AB/MDS Sciex) that was interfaced to a nanoscale, reverse-phase, high-pressure, liquid chromatograph (Tempo) using a 10 cm-180 ID glass capillary packed with 5-μm C18 ZorbaxTM beads (Agilent). Buffer compositions were as follows: Buffer A — 98% H_2O, 2% ACN, 0.2% formic acid, and 0.005% TFA; Buffer B — 100% ACN, 0.2% formic acid, and 0.005% TFA. Peptides were eluted from the C-18 column into the mass spectrometer using a linear gradient of 5–60% Buffer B over 60 min at 400 mL/min. LC–MS/MS data were acquired in a data-dependent fashion by selecting the four most intense peaks with charge states of 2 to 4 that exceed 20 counts, with exclusion of former target ions set to "360 s" and the mass tolerance for exclusion set to 100 ppm. Time-of-flight MS were acquired at *m/z* 400 to 1600 Da for 1 s with summation of 12 time bins. MS/MS data were acquired from *m/z* 50 to 2000 Da by using "enhance all" (24 time bins summed), dynamic background subtract, automatic collision energy, and automatic MS/MS accumulation with the fragment intensity multiplier set to 6 and maximum accumulation set to 2 s before returning to the survey scan. Peptide identifications were made using the paragon algorithm executed in Protein Pilot 2.0 (Life Technologies).

Heat titration of assembly products

Samples containing procapsids and phage were incubated for 15 min in an Applied Biosystems GeneAmp thermalcycler at temperatures ranging from 20 to 90 °C, after which they were placed on ice and diluted with ice-cold agarose sample buffer. Electrophoresis was performed at room temperature in TAE buffer with 110 V for 90–120 min.

Construction of Shigella omp null mutants

The sequences of the *ompA* and *ompC* genes and nearby surrounding regions are virtually identical in the reported *E. coli* K-12 and *S. flexneri* 2a strain 301 genome sequences (strain 301 locus_tagss SF0957 and SF2299, respectively) (Blattner et al., 1997; Jin et al., 2002). *E. coli* K-12 mutants of these genes exist in the Kieo collection (strains JM0940 and JM2203, respectively) in which a kanamycin resistance cassette replaces the gene (Baba et al., 2006). We used polymerase chain reaction (PCR) to amplify approximately 2 kbp regions that include the *ompA* and *ompC* replacements from these two strains with oligonucleotide pairs 5′-ATCTGGTGAAGAAGCATCGCGAAGGGGAG/5′-AACGCTATGGGGTTTATTATGCGTCCGG and 5′-GGCTGTTGTTCCGGGCCAAAG/5′-GTAATAAATAAAGTTAATGATGATAGCG, respectively. The resulting DNA was used to electroporate *S. flexneri* strain PE577 that carried plasmid pKD46 (Datsenko and Wanner, 2000), kanamycin resistant transformants were selected, and pKD46 was removed by growth at 40 °C. The presence of the properly placed resistance cassette in the resulting kanamycin resistant *Shigella* transformants was confirmed by PCR amplification and sequencing of the amplified DNA across all kanamycin cassette insertion boundaries.

Acknowledgments

We thank N. Olson for expert guidance in cryoEM methods, K. and J. Pogliano (UCSD) for access to equipment and lab space, Debbie Ang (U of Utah) for *E. coli* strains, R. Khayat and J.E. Johnson (Scripps Research Institute) for helpful discussions, G. Lander (UC Berkeley) for the segmented P22 gp10 cryoEM density map, and G. Cingolani (Thomas Jefferson U) for the homology model of the Sf6 tail needle. We also thank C. Teschke (UConn) for helpful suggestions and use of lab space and A. Yashchenko for help with image digitization and preliminary data processing. This work was supported in part by NIH grants R37 GM-033050 and 1S10 RR-020016 to TSB, AI074825 to SRC, NIH fellowship F32A1078624 to KNP, and support from UCSD and the Agouron Foundation to TSB to establish and support the UCSD cryoEM facilities.

References

Agirrezabala, X., Martin-Benito, J., Caston, J.R., Miranda, R., Valpuesta, J.M., Carrascosa, J.L., 2005. Maturation of phage T7 involves structural modification of both shell and inner core components. EMBO J. 24, 3820–3829.

Allison, G.E., Verma, N.K., 2000. Serotype-converting bacteriophages and O-antigen modification in *Shigella flexneri*. Trends Microbiol. 8, 17–23.

Andres, D., Hanke, C., Baxa, U., Seul, A., Barbirz, S., Seckler, R., 2010. Tailspike interactions with lipopolysaccharide effect DNA ejection from phage P22 particles in vitro. J. Biol. Chem. 285, 36768–36775.

Baba, T., Ara, T., Hasegawa, M., Takai, Y., Okumura, Y., Baba, M., Datsenko, K.A., Tomita, M., Wanner, B.L., Mori, H., 2006. Construction of *Escherichia coli* K-12 in-frame, single-gene knockout mutants: the Keio collection. Mol. Syst. Biol. 2, 2006 0008.

Baker, T.S., Olson, N.H., Fuller, S.D., 1999. Adding the third dimension to virus life cycles: three-dimensional reconstruction of icosahedral viruses from cryo-electron micrographs. [erratum appears in Microbiol Mol Biol Rev 2000 64:237.]. Microbiol. Mol. Biol. Rev. 63, 862–922.

Baker, M.L., Jiang, W., Rixon, F.J., Chiu, W., 2005. Common ancestry of herpesviruses and tailed DNA bacteriophages. J. Virol. 79, 14967–14970.

Bamford, D.H., Grimes, J.M., Stuart, D.I., 2005. What does structure tell us about virus evolution? Curr. Opin. Struct. Biol. 15, 655–663.

Banks, D.J., Beres, S.B., Musser, J.M., 2002. The fundamental contribution of phages to GAS evolution, genome diversification and strain emergence. Trends Microbiol. 10, 515–521.

Basle, A., Rummel, G., Storici, P., Rosenbusch, J.P., Schirmer, T., 2006. Crystal structure of osmoporin OmpC from *E. coli* at 2.0 A. J. Mol. Biol. 362, 933–942.

Bhardwaj, A., Molineux, I.J., Casjens, S.R., Cingolani, G., 2011. Atomic structure of bacteriophage Sf6 tail needle knob. J. Biol. Chem. 286, 30867–30877.

Blattner, F.R., Plunkett 3rd, G., Bloch, C.A., Perna, N.T., Burland, V., Riley, M., Collado-Vides, J., Glasner, J.D., Rode, C.K., Mayhew, G.F., Gregor, J., Davis, N.W., Kirkpatrick, H.A., Goeden, M.A., Rose, D.J., Mau, B., Shao, Y., 1997. The complete genome sequence of *Escherichia coli* K-12. Science 277, 1453–1462.

Bowman, V.D., Chase, E.S., Franz, A.W., Chipman, P.R., Zhang, X., Perry, K.L., Baker, T.S., Smith, T.J., 2002. An antibody to the putative aphid recognition site on cucumber mosaic virus recognizes pentons but not hexons. J. Virol. 76, 12250–12258.

Boyd, E.F., Brussow, H., 2002. Common themes among bacteriophage-encoded virulence factors and diversity among the bacteriophages involved. Trends Microbiol. 10, 521–529.
Broadbent, S.E., Davies, M.R., van der Woude, M.W., 2010. Phase variation controls expression of *Salmonella* lipopolysaccharide modification genes by a DNA methylation-dependent mechanism. Mol. Microbiol. 77, 337–353.
Brown, J.C., Newcomb, W.W., 2011. Herpesvirus capsid assembly: insights from structural analysis. Curr. Opin. Virol. 1, 142–149.
Canchaya, C., Fournous, G., Brussow, H., 2004. The impact of prophages on bacterial chromosomes. Mol. Microbiol. 53, 9–18.
Casjens, S.R., 2005. Comparative genomics and evolution of the tailed-bacteriophages. Curr. Opin. Microbiol. 8, 451–458.
Casjens, S., Hendrix, R., 2005. Bacteriophages and the bacterial genome. In: Higgins, N.P. (Ed.), The Bacterial Chromosome. ASM Press, Washington D.C., pp. 39–52.
Casjens, S., Molineux, I., 2012. Short non-contractile tail machines: adsorption and DNA delivery by the podoviruses. In: Rossmann, M., Rao, V. (Eds.), Viral Molecular Machines, Adv. Exp. Med. Biol., vol. 726, pp. 143–179.
Casjens, S.R., Thuman-Commike, P.A., 2011. Evolution of mosaically related tailed bacteriophage genomes seen through the lens of phage P22 virion assembly. Virology 411, 393–415.
Casjens, S., Weigele, P., 2005. Headful DNA packaging by bacteriophage P22. In: Catalano, C. (Ed.), Viral Genome Packaging Machines. Landes Bioscience, Georgetown, TX, pp. 80–88.
Casjens, S., Adams, M.B., Hall, C., King, J., 1985. Assembly-controlled autogenous modulation of bacteriophage P22 scaffolding protein gene expression. J. Virol. 53, 174–179.
Casjens, S., Winn-Stapley, D.A., Gilcrease, E.B., Morona, R., Kuhlewein, C., Chua, J.E., Manning, P.A., Inwood, W., Clark, A.J., 2004. The chromosome of *Shigella flexneri* bacteriophage Sf6: complete nucleotide sequence, genetic mosaicism, and DNA packaging. J. Mol. Biol. 339, 379–394.
Cerritelli, M.E., Studier, F.W., 1996. Assembly of T7 capsids from independently expressed and purified head protein and scaffolding protein. J. Mol. Biol. 258, 286–298.
Chang, J.T., Schmid, M.F., Haase-Pettingell, C., Weigele, P.R., King, J.A., Chiu, W., 2010. Visualizing the structural changes of bacteriophage Epsilon15 and its *Salmonella* host during infection. J. Mol. Biol. 402, 731–740.
Cheetham, B.F., Katz, M.E., 1995. A role for bacteriophages in the evolution and transfer of bacterial virulence determinants. Mol. Microbiol. 18, 201–208.
Chen, D.H., Baker, M.L., Hryc, C.F., DiMaio, F., Jakana, J., Wu, W., Dougherty, M., Haase-Pettingell, C., Schmid, M.F., Jiang, W., Baker, D., King, J.A., Chiu, W., 2011. Structural basis for scaffolding-mediated assembly and maturation of a dsDNA virus. Proc. Natl. Acad. Sci. U.S.A. 108, 1355–1360.
Clark, C.A., Beltrame, J., Manning, P.A., 1991. The oac gene encoding a lipopolysaccharide O-antigen acetylase maps adjacent to the integrase-encoding gene on the genome of *Shigella flexneri* bacteriophage Sf6. Gene 107, 43–52.
Conway, J.F., Duda, R.L., Cheng, N., Hendrix, R.W., Steven, A.C., 1995. Proteolytic and conformational control of a virus capsid maturation: the bacteriophage HK97 system. J. Mol. Biol. 253, 86–99.
Datsenko, K.A., Wanner, B.L., 2000. One-step inactivation of chromosomal genes in *Escherichia coli* K-12 using PCR products. Proc. Natl. Acad. Sci. U.S.A. 97, 6640–6645.
Dokland, T., Murialdo, H., 1993. Structural transitions during maturation of bacteriophage lambda capsids. J. Mol. Biol. 233, 682–694.
Gasteiger, E., Hoogland, C., Gattiker, A., Duvaud, S., Wilkins, M.R., Appel, R.D., Bairoch, A., 2005. Protein identification and analysis tools on the ExPASy server. In: Walker, J.M. (Ed.), The Proteomics Protocols Handbook. Humana Press, pp. 571–607.
Gemski Jr., P., Koeltzow, D.E., Formal, S.B., 1975. Phage conversion of *Shigella flexneri* group antigens. Infect. Immun. 11, 685–691.
Gertsman, I., Gan, L., Guttman, M., Lee, K., Speir, J.A., Duda, R.L., Hendrix, R.W., Komives, E.A., Johnson, J.E., 2009. An unexpected twist in viral capsid maturation. Nature 458, 646–650.
Gertsman, I., Fu, C.Y., Huang, R., Komives, E.A., Johnson, J.E., 2010. Critical salt bridges guide capsid assembly, stability, and maturation behavior in bacteriophage HK97. Mol. Cell. Proteomics 9, 1752–1763.
Gilcrease, E.B., Winn-Stapley, D.A., Hewitt, F.C., Joss, L., Casjens, S.R., 2005. Nucleotide sequence of the head assembly gene cluster of bacteriophage L and decoration protein characterization. J. Bacteriol. 187, 2050–2057.
Goddard, T.D., Huang, C.C., Ferrin, T.E., 2007. Visualizing density maps with UCSF Chimera. J. Struct. Biol. 157, 281–287.
Hendrix, R.W., 2002. Bacteriophages: evolution of the majority. Theor. Popul. Biol. 61, 471–480.
Ho, T.D., Slauch, J.M., 2001. OmpC is the receptor for Gifsy-1 and Gifsy-2 bacteriophages of *Salmonella*. J. Bacteriol. 183, 1495–1498.
Huang, R.K., Khayat, R., Lee, K.K., Gertsman, I., Duda, R.L., Hendrix, R.W., Johnson, J.E., 2011. The Prohead-I structure of bacteriophage HK97: implications for scaffold-mediated control of particle assembly and maturation. J. Mol. Biol. 408, 541–554.
Ionel, A., Velazquez-Muriel, J.A., Luque, D., Cuervo, A., Caston, J.R., Valpuesta, J.M., Martin-Benito, J., Carrascosa, J.L., 2011. Molecular rearrangements involved in the capsid shell maturation of bacteriophage T7. J. Biol. Chem. 286, 234–242.
Jaroszewski, L., Rychlewski, L., Li, Z., Li, W., Godzik, A., 2005. FFAS03: a server for profile–profile sequence alignments. Nucl. Acids Res. 33.
Jiang, W., Baker, M.L., Jakana, J., Weigele, P.R., King, J., Chiu, W., 2008. Backbone structure of the infectious ε15 virus capsid revealed by electron cryomicroscopy. Nature 451, 1130–1134.
Jin, Q., Yuan, Z., Xu, J., Wang, Y., Shen, Y., Lu, W., Wang, J., Liu, H., Yang, J., Yang, F., Zhang, X., Zhang, J., Yang, G., Wu, H., Qu, D., Dong, J., Sun, L., Xue, Y., Zhao, A., Gao, Y., Zhu, J., Kan, B., Ding, K., Chen, S., Cheng, H., Yao, Z., He, B., Chen, R., Ma, D., Qiang, B., Wen, Y., Hou, Y., Yu, J., 2002. Genome sequence of *Shigella flexneri* 2a: insights into pathogenicity through comparison with genomes of *Escherichia coli* K12 and O157. Nucleic Acids Res. 30, 4432–4441.
Johnson, J.E., Chiu, W., 2007. DNA packaging and delivery machines in tailed bacteriophages. Curr. Opin. Struct. Biol. 17, 237–243.
King, J., Casjens, S., 1974. Catalytic head assembling protein in virus morphogenesis. Nature 251, 112–119.
King, M.R., Vimr, R.P., Steenbergen, S.M., Spanjaard, L., Plunkett 3rd, G., Blattner, F.R., Vimr, E.R., 2007. *Escherichia coli* K1-specific bacteriophage CUS-3 distribution and function in phase-variable capsular polysialic acid O acetylation. J. Bacteriol. 189, 6447–6456.
Koebnik, R., Locher, K.P., Van Gelder, P., 2000. Structure and function of bacterial outer membrane proteins: barrels in a nutshell. Mol. Microbiol. 37, 239–253.
Kotloff, K.L., Winickoff, J.P., Ivanoff, B., Clemens, J.D., Swerdlow, D.L., Sansonetti, P.J., Adak, G.K., Levine, M.M., 1999. Global burden of *Shigella* infections: implications for vaccine development and implementation of control strategies. Bull. World Health Organ. 77, 651–666.
Lander, G.C., Tang, L., Casjens, S.R., Gilcrease, E.B., Prevelige, P.J., Poliakov, A., Potter, C.S., Carragher, B., Johnson, J.E., 2006. The structure of an infectious P22 virion shows the signal for headful DNA packaging. Science 312, 1791–1795.
Lander, G.C., Evilevitch, A., Jeemaeva, M., Potter, C.S., Carragher, B., Johnson, J.E., 2008. Bacteriophage lambda stabilization by auxiliary protein gpD: timing location, and mechanism of attachment determined by cryo-EM. Structure 16, 1399–1406.
Lander, G.C., Khayat, R., Li, R., Prevelige, P.J., Potter, C.S., Carragher, B., Johnson, J.E., 2009. The P22 tail machine at subnanometer resolution reveals the architechture of an infectious conduit. Structure 17, 789–799.
Liu, B., Knirel, Y.A., Feng, L., Perepelov, A.V., Senchenkova, S.N., Wang, Q., Reeves, P.R., Wang, L., 2008. Structure and genetics of *Shigella* O antigens. FEMS Microbiol. Rev. 32, 627–653.
Liu, X., Zhang, Q., Murata, K., Baker, M.L., Sullivan, M.B., Fu, C., Dougherty, M.T., Schmid, M.F., Osburne, M.S., Chisholm, S.W., Chiu, W., 2010. Structural changes in a marine podovirus associated with release of its genome into *Prochlorococcus*. Nat. Struct. Mol. Biol. 17, 830–837.
McGuffin, L.J., Bryson, K., Jones, D.T., 2000. The PSIPRED protein structure prediction server. Bioinformatics 16, 404–405.
Mindell, J.A., Grigorieff, N., 2003. Accurate determination of local defocus and specimen tilt in electron microscopy. J. Struct. Biol. 142, 334–347.
Morais, M.C., Choi, K.H., Koti, J.S., Chipman, P.R., Anderson, D.L., Rossmann, M.G., 2005. Conservation of the capsid structure in the tailed dsDNA bacteriophages: the pseudoatomic structure of φ29. Mol. Cell 18, 149–159.
Morona, R., Klose, M., Henning, U., 1984. *Escherichia coli* K-12 outer membrane protein (OmpA) as a bacteriophage receptor: analysis of mutant genes expressing altered proteins. J. Bacteriol. 159, 570–578.
Morona, R., Mavris, M., Fallarino, A., Manning, P.A., 1994. Characterization of the rfc region of *Shigella flexneri*. J. Bacteriol. 176, 733–747.
Muller, J.J., Barbirz, S., Heinle, K., Freiberg, A., Seckler, R., Heinemann, U., 2008. An intersubunit active site between supercoiled parallel beta helices in the trimeric tailspike endorhamnosidase of *Shigella flexneri* phage Sf6. Structure 16, 766–775.
Olia, A.S., Prevelige Jr., P.E., Johnson, J.E., Cingolani, G., 2011. Three-dimensional structure of a viral genome-delivery portal vertex. Nat. Struct. Mol. Biol. 18, 597–603.
Parent, K.N., Khayat, R., Tu, L.H., Suhanovsky, M.M., Cortines, J.R., Teschke, C.M., Johnson, J.E., Baker, T.S., 2010a. P22 coat protein structures reveal a novel mechanism for capsid maturation: stability without auxiliary proteins or chemical crosslinks. Structure 18, 390–410.
Parent, K.N., Sinkovits, R.S., Suhanovsky, M.M., Teschke, C.M., Egelman, E.H., Baker, T.S., 2010b. Cryo-reconstructions of P22 polyheads suggest that phage assembly is nucleated by trimeric interactions among coat proteins. Phys. Biol. 7, 045004.
Pautsch, A., Schulz, G.E., 2000. High-resolution structure of the OmpA membrane domain. J. Mol. Biol. 298, 273–282.
Prasad, B.V.V., Prevelige Jr., P.E., Marieta, E., Chen, R.O., Thomas, D., King, J., Chiu, W., 1993. Three-dimensional transformation of capsids associated with genome packaging in a bacterial virus. J. Mol. Biol. 231, 65–74.
Prevelige, P.E., 2006. Bacteriophage P22. The Bacteriophages (Calendar, R., Ed.), 2nd edition. Oxford University Press. p457–468.
Prevelige Jr., P.E., King, J., 1993. Assembly of bacteriophage P22: a model for ds-DNA virus assembly. Prog. Med. Virol. 40, 206–221.
Raytcheva, D.A., Haase-Pettingell, C., Piret, J.M., King, J.A., 2011. Intracellular assembly of cyanophage Syn5 proceeds through a scaffold-containing procapsid. J. Virol. 85, 2406–2415.
Serwer, P., Pichler, M.E., 1978. Electrophoresis of bacteriophage T7 and T7 capsids in agarose gels. J. Virol. 28, 917–928.
Sondermann, P., Huber, R., Oosthuizen, V., Jacob, U., 2000. The 3.2-A crystal structure of the human IgG1 Fc fragment-Fc gammaRIII complex. Nature 406, 267–273.
Spilman, M.S., Dearborn, A.D., Chang, J.R., Damle, P.K., Christie, G.E., Dokland, T., 2011. A conformational switch involved in maturation of *Staphylococcus aureus* bacteriophage 80α capsids. J. Mol. Biol. 405, 863–876.
Steinbacher, S., Seckler, R., Miller, S., Steipe, B., Huber, R., Reinemer, P., 1994. Crystal structure of P22 tailspike protein: interdigitated subunits in a thermostable trimer. Science 265, 383–386.
Sternberg, N., Weisberg, R., 1977. Packaging of coliphage lambda DNA. II. The role of the gene D protein. J. Mol. Biol. 117, 733–759.
Suhanovsky, M.M., Parent, K.N., Dunn, S.E., Baker, T.S., Teschke, C.M., 2010. Determinants of bacteriophage P22 polyhead formation: the role of coat protein flexibilty in conformational switching. Mol. Microbiol. 77, 1568–1582.
Sun, Y., Parker, M.H., Weigele, P., Casjens, S., Prevelige, P.E.J., Krishna, N.R., 2000. Structure of the coat protein-binding domain of the scaffolding protein from a double-stranded DNA virus. J. Mol. Biol. 297, 1195–1202.

Tang, L., Gilcrease, E.B., Casjens, S.R., Johnson, J.E., 2006. Highly discriminatory binding of capsid cementing protiens in bacteriophage L. Structure 14, 837–845.
Tang, J., Olson, N., Jardine, P.J., Grimes, S., Anderson, D.L., Baker, T.S., 2008. DNA poised for release in bacteriophage φ29. Structure 16, 935–943.
Tang, J., Lander, G.C., Olia, A., Li, R., Casjens, S., Prevelige Jr., P., Cingolani, G., Baker, T.S., Johnson, J.E., 2011. Peering down the barrel of a bacteriophage portal: the genome packaging and release valve in P22. Structure 19, 496–502.
Tanji, Y., Hattori, K., Suzuki, K., Miyanaga, K., 2008. Spontaneous deletion of a 209-kilobase-pair fragment from the *Escherichia coli* genome occurs with acquisition of resistance to an assortment of infectious phages. Appl. Environ. Microbiol. 74, 4256–4263.
Teschke, C.M., Parent, K.N., 2010. 'Let the phage do the work': using the phage P22 coat protein structure as a framework to understand its folding and assembly mutants. Virology 401, 119–130.
Teschke, C.M., McGough, A., Thuman-Commike, P.A., 2003. Penton release from P22 heat-expanded capsids suggests importance of stabilizing penton–hexon interactions during capsid maturation. Biophys. J. 84, 2585–2592.
Thuman-Commike, P.A., Greene, B., Jokana, J., Prasad, B.V.V., King, J., Prevelige Jr., P.E., Chiu, W., 1996. Three-dimensional structure of scaffolding-containing phage P22 procapsids by electron cryo-microscopy. J. Mol. Biol. 260, 85–98.
Trus, B.L., Booy, F.P., Newcomb, W.W., Brown, J.C., Homa, F.L., Thomsen, D.R., Steven, A.C., 1996. The herpes simplex virus procapsid: structure, conformational changes upon maturation, and roles of the triplex proteins VP19c and VP23 in assembly. J. Mol. Biol. 263, 447–462.
van Heel, M., Schatz, M., 2005. Fourier shell correlation threshold criteria. J. Struct. Biol. 151, 250–262.
Verma, N.K., Brandt, J.M., Verma, D.J., Lindberg, A.A., 1991. Molecular characterization of the O-acetyl transferase gene of converting bacteriophage SF6 that adds group antigen 6 to *Shigella flexneri*. Mol. Microbiol. 5, 71–75.
Wikoff, W.R., Duda, R.L., Hendrix, R.W., Johnson, J.E., 1999. Crystallographic analysis of the dsDNA bacteriophage HK97 mature empty capsid. Acta Crystallogr. D Biol. Crystallogr. 55, 763–771.
Wikoff, W.R., Liljas, L., Duda, R.L., Tsuruta, H., Hendrix, R.W., Johnson, J.E., 2000. Topologically linked protein rings in the bacteriophage HK97 capsid. Science 289, 2129–2133.
Yan, X., Dryden, K.A., Tang, J., Baker, T.S., 2007a. Ab initio random model method facilitates 3D reconstruction of icosahedral particles. J. Struct. Biol. 157, 211–225.
Yan, X., Sinkovits, R.S., Baker, T.S., 2007b. AUTO3DEM—an automated and high throughput program for image reconstruction of icosahedral particles. J. Struct. Biol. 157, 73–82.
Yang, F., Yang, J., Zhang, X., Chen, L., Jiang, Y., Yan, Y., Tang, X., Wang, J., Xiong, Z., Dong, J., Xue, Y., Zhu, Y., Xu, X., Sun, L., Chen, S., Nie, H., Peng, J., Xu, J., Wang, Y., Yuan, Z., Wen, Y., Yao, Z., Shen, Y., Qiang, B., Hou, Y., Yu, J., Jin, Q., 2005. Genome dynamics and diversity of *Shigella* species, the etiologic agents of bacillary dysentery. Nucleic Acids Res. 33, 6445–6458.
Yang, Q., Maluf, N.K., Catalano, C.E., 2008. Packaging of a unit-length viral genome: the role of nucleotides and the gpD decoration protein in stable nucleocapsid assembly in bacteriophage lambda. J. Mol. Biol. 383, 1037–1048.
Yu, F., Mizushima, S., 1982. Roles of lipopolysaccharide and outer membrane protein OmpC of *Escherichia coli* K-12 in the receptor function for bacteriophage T4. J. Bacteriol. 151, 718–722.
Zhao, H., Finch, C.J., Sequeira, R.D., Johnson, B.A., Johnson, J.E., Casjens, S.R., Tang, L., 2010. Crystal structure of the DNA-recognition component of the bacterial virus Sf6 genome-packaging machine. Proc. Natl. Acad. Sci. U.S.A. 107, 1971–1976.
Zhao, H., Sequeira, R.D., Galeva, N.A., Tang, L., 2011. The host outer membrane proteins OmpA and OmpC are associated with the *Shigella* phage Sf6 virion. Virology 409, 319–327.
Zinder, N.D., Lederberg, J., 1952. Genetic exchange in *Salmonella*. J. Bacteriol. 64, 679–699.